Applied Surface Science 551 (2021) 149304

Contents lists available at ScienceDirect

Applied Surface Science

journal homepage: www.elsevier.com/locate/apsusc

Full Length Article

Computational insight of ZrS_2/graphene heterobilayer as an efficient anode material

Shafiq Ur Rehman [a], Abdus Samad [b], Muhammad Saeed [c], Bin Amin [d], Muhammad Hafeez [a], Irshad A. Mir [a], ling Zhu [a,*]

[a] College of Physics and Optoelectronic Engineering, Shenzhen University, Nanhai Ave. 3688, Shenzhen, Guangdong 518060, People's Republic of China
[b] Department of Physics, University of Ulsan, Ulsan 44610, Republic of Korea
[c] College of Nuclear Science and Engineering, East China University of Technology, Nanchang 330013, China
[d] Department of Physics, Abbottabad University of Science and Technology, Abbottabad 22010, Pakistan

ARTICLE INFO

Keywords:
Density functional theory
Graphene
monolayer ZrS_2
ZrS_2/graphene
Specific capacity
Open circuit voltage
Activation energy barrier

ABSTRACT

A density functional theory-based study is carried out to examine the electrochemical performance of ZrS_2 and graphene monolayers and ZrS_2/graphene heterobilayer for anodic applications in rechargeable Li ion batteries (LIBs). The energetic and dynamic stabilities of the heterobilayer have been confirmed first. The low Li diffusion barrier (0.24 eV), low half-cell voltage (0.7 V) and high Li storage capacity (700 mAh/g) of ZrS_2 monolayer makes it a prospective 2D anode material for the LIBs. However, the large energy gap of ZrS_2 monolayer may reduce the reversibility, while large structural changes are on high Li load can lead to short cycle life. To handle these issues, the ZrS_2 monolayer is capped with graphene. The graphene thus provides mechanical strength and conducting channels to the electron flow. It is well known that graphene is unable to store Li for LIBs applications. However, by making its interface with ZrS_2 enables it to store Li ion reversibly. Furthermore, the graphene caping provides mechanical strength to the ZrS_2 monolayer to insure long cycle life and high recyclability. Thus, the hybrid of ZrS_2 and graphene makes a highly efficient 2D anode material for Li ion batteries.

1. Introduction

Rechargeable Li ion battery (LIB) technology is playing the role of backbone in the modern electronics industry. Owing to their high energy and power density, clean energy storage and long cycle life, LIBs have many applications [1–9]. Currently, LIBs are used in portable electronic devices, such as mobile phone, laptop computer, and green grids [10–13]. The electrochemical performance of a LIB is highly dependent on the choice of their electrode materials. Therefore, appropriate electrode materials are to be searched out to enhance the specific capacity, cell voltage, Li kinetics, and cycle life [5,14,15]. In this regard, many efforts have been made to investigate proper anode materials for the better and better performance of LIBs [6,16–18]. The excellent electrical and thermal conductivity, high electrochemical potential, high mechanical strength, dynamic stability, and low cost make graphene a potential candidate for the applications in LIBs [1,4]. However, the Li adsorption energy of graphene is too low to avoid the Li dendrite formation. Many two dimensional (2D) materials like silicene, transition metal dichalcogenides (TMDs), and MXenes have shown a high potential to be used as anode materials in LIBs [7–10]. Although the TMDs have high Li storage capacity and low Li diffusion barriers, they are insulators and have a low electronic conductivity which limits the electrochemical performance of a battery [19,20]. Similarly, the doping strategies in graphene can increase the Li storage capacity to 2900 mAh/g but on the other side they may lower the charging rate of a battery [4,19]. Recently, researches for finding new class of 2D semiconductor (e.g. MoS_2, WS_2, $MoSe_2$, Mo_2C, W_2C, TiS_2, SnS_2, GeS, GaS and ZrS_2) monolayers have been a hot topic owing to their potential applications in the field of optoelectronics, energy harvesting, gas sensors, catalysis, field effect transistors and storage devices [5,12,21–26]. These nanoscale materials have astonishing behavior, such as tunable electronic energy gap, high optical absorption and high mechanical strength, which makes them superior in the microelectronic industry [5,19,27]. The semiconductor monolayer materials are best considered for the rechargeable batteries as anode materials. For example, Mo_2C and W_2C monolayers are studied very recently for their metallic nature, high mechanical strength, thermal and dynamic stability, and high charge capacity; it is proved that these transition metal carbides are promising candidates for

* Corresponding author.
E-mail address: zhuling@szu.edu.cn (Zhu).

https://doi.org/10.1016/j.apsusc.2021.149304
Received 25 June 2020; Received in revised form 17 January 2021; Accepted 9 February 2021
Available online 14 February 2021

the LIBs [5,19]. Similarly, other monolayers, MoS_2, $MoSe_2$, TiS_2 and SnS_2 etc., are also synthesized experimentally and studied theoretically as well, and their applications to the LIBs have been extensively investigated [11,28–32]. It is shown experimentally that MoS_2 has a high storage capacity and is considered as a promising anode material for the LIBs [33,34]. First-principles calculations have also shown that MoS_2 monolayer has high adsorption energy and low energy barrier [35].

Although the above mentioned 2D materials show a high potential for Li ion batteries application, electronic conductivity, the number of intercalation sites and stability are also crucial properties for building high-performance energy storage devices. While isolated 2D materials, such as graphene, can show some of the required properties, none of them can offer all properties to maximize energy density, power density, and cycle life [36]. Furthermore, the irregular surface morphology and dangling bonds at the surface of single-layer materials make it unstable and reduction of their electronic conductivity and hence can limit their effective use as electrodes [37]. To overcome these limitations and to make the single-layer materials more useful candidate for the energy storage application, the isolated monolayers are combined into heterostructures [36]. With the rapid development in the nanotechnology more and more van der Waals heterostructures have been investigated and have shown combined properties [27,37–40]. Furthermore, several theoretical and experimental reports have shown that combining the graphene (with high electrical conductivity) and transition metal (high redox activity) into stacked 2D heterostructure can enhance the electrochemical performance of a battery due to synergistic interactions [12,38–40]. MoS_2 in junction with graphene has been widely studied, but due to low electrical conductivity, MoS_2 cannot fulfill the demand of high electrical conductivity. Graphene/silicene heterostructure has been studied by the first principles calculations for the application of Li and Na ion batteries; it has shown better performances, such as, high storage capacity (487 mAh/g), low activation energy barrier (0.4 eV), and high binding strength for Li and Na ions than the pristine silicene [41]. Similarly, SnS_2/graphene, VS_2/graphene, and VS_2/MoS_2 heterostructures have been predicted as the best anode material for LIBs, because of its highly enhanced electrochemical performances, such as good electronic mobility, excellent electrical conductivity, high charge storage capacity, low half-cell voltage, and low activation energy barrier [12,42,43].

Recently, ZrS_2 (1200 $cm^2\ V^{-1}\ S^{-1}$) monolayer has been realized to have electronic mobility much higher than MoS_2 (400 $cm^2\ V^{-1}\ S^{-1}$) along with high in-plane stiffness 75.74 N/m [44–49]. Low Li storage capacity, volume variations during the lithiation/delithiation process, and lack of electrical conductivity are the main issues in the electrode materials of a rechargeable LIB. The ZrS_2 monolayer has a high Li binding energy but it has low mechanical strength and high band gap. On the other hand, graphene has high electrical conductivity and high mechanical strength but it has a low Li binding energy. Although these materials in individual are not efficient for electrochemistry but their heterostructure can cover all the deficiencies to make an ideal anode for LIBs. We expect that our findings of ZrS_2/graphene heterostructure as anode for LIBs can play a leading role for the electrochemists in finding advanced anode materials.

In the present work, ZrS_2 monolayer is considered as an anode material for application to LIBs. We have found that ZrS_2 monolayer is chemically very active for the Li ion adsorption possessing higher binding energies for the Li ions. The open-circuit voltage (OCV), specific capacity, and activation energy barrier for ZrS_2 monolayer are 0.7 V, 700 mAh/g, and 0.24 eV, respectively. However, ZrS_2 monolayer is semiconducting whereas a metallicity is one of the important parameters for anode materials. More than that, large structural variations are noticed at high Li capacity. The ZrS_2 monolayer is decomposed to Li_2S and Zr at high Li concentrations which could decrease cycle life of the anode. It also makes the Li reversibility impossible. On the other hand, graphene is reported as poor anode materials for LIBs, because of its weak Li binding. However, being a metal with high mechanical stiffness, it could be combined with the ZrS_2 monolayer to make a perfect 2D anode material. Interestingly, the ZrS_2/graphene heterobilayer solves all these issues. The graphene provide mechanical strength and electron conducting channels while the interfacial charge redistribution makes it viable to store Li on the graphene surface. Thus, constructing the ZrS_2 and graphene contact for LIBs anode turns out to be a good strategy which could help the experimentalists in search of next generation LIBs anode materials.

2. Computational details

We used a quantum mechanical approach by density functional theory (DFT) implemented in the VASP (Vienna Ab Initio Simulation Package) code with the generalized gradient approximation (GGA) and Perdew-Burke-Ernzerhof (PBE) functional for the electron exchange correlation [50,51]. We also used the HSE06 functional for the electronic structure calculations of ZrS_2 monolayer [52]. The plane wave cut-off energy was chosen as 450 eV for the ZrS_2 monolayer and 600 eV for the ZrS_2/graphene heterostructure. The (4d, 5p) and (2s,4p) were treated as valence states in the Zr and S atoms, respectively. The ZrS_2 monolayer and ZrS_2/graphene heterostructure were relaxed with the force criteria of 0.01 eV $Å^{-1}$. A vacuum of 26 Å was applied along the *c*-direction to avoid the self-interactions in the monolayer case. *k*-mesh of $7 \times 7 \times 1$ was used in the relaxation for ZrS_2 monolayer and of $5 \times 5 \times 1$ for ZrS_2/graphene heterostructure [53]. A $2 \times 2 \times 1$ supercell of ZrS_2 monolayer was considered for calculating the Li adsorption capacity. To reduce the lattice mismatch between the ZrS_2 monolayer and graphene we combine the $2 \times 2 \times 1$ supercell of ZrS_2 with a $3 \times 3 \times 1$ supercell of graphene to make ZrS_2/graphene heterostructure. In the heterostructure, we take into account the van der Waals interaction by using DFT-D2 scheme (Grime approach of van der Waals interaction) [54]. The climbed image nudged elastic band (CI-NEB) method was used to study the minimum energy path for the Li diffusion from one favorable adsorption site to another favorable adsorption site on the surface of ZrS_2 monolayer and ZrS_2/graphene heterobilayer and find the saddle points [55,56]. This method is a reliable tool for finding the activation energy barrier and minimum energy path (MEP) between the two stable states. We perform it by the linear interpolation of five intermediate images between the two stable adsorption sites of Li. The dynamic stability of ZrS_2 monolayer was checked with the finite displacement method, implemented in the Phonopy code [57].

3. Results and discussion

3.1. ZrS_2 monolayer

We first built the bulk structures of ZrS_2 in two different phases, i.e. 2H phase and 1T phase, with space groups (*P63/mmc*) and ($P3m_1$), respectively, and then converted each structure into pristine monolayers by producing a vacuum of 20 Å along the out-of-plane direction. These structures were fully relaxed to optimize the structural parameters. By comparing the total energies of the 1T and 2H phases of the monolayer ZrS_2, we found that the 1T phase of ZrS_2 is energetically more stable by 540 meV/formula unit than its 2H phase. We therefore study the 1T phase of the monolayer ZrS_2 for Li adsorption. The optimized lattice parameters for the 1T phase of monolayer ZrS_2 are $a = b = 2.84$ Å and the bond length of Zr-S is 2.16 Å, in good agreement with literature [48,49]. A $3 \times 3 \times 1$ supercell of the 1T-ZrS_2 monolayer is shown in Fig. 1. The dynamic stability was investigated with phonon lattice vibrations calculations. The absence of soft modes in the phonon dispersion curves over the entire Brillion zone in Fig. 2(a) shows that the 1T phase is stable dynamically. Fig. 2(b) shows the electronic band structure and total density of states (TDOS) of the ZrS_2 monolayer calculated with HSE06 functional. It reveals that the monolayer ZrS_2 is a semiconductor with energy gap of 1.1 eV; the results are in good agreement with literature [48].

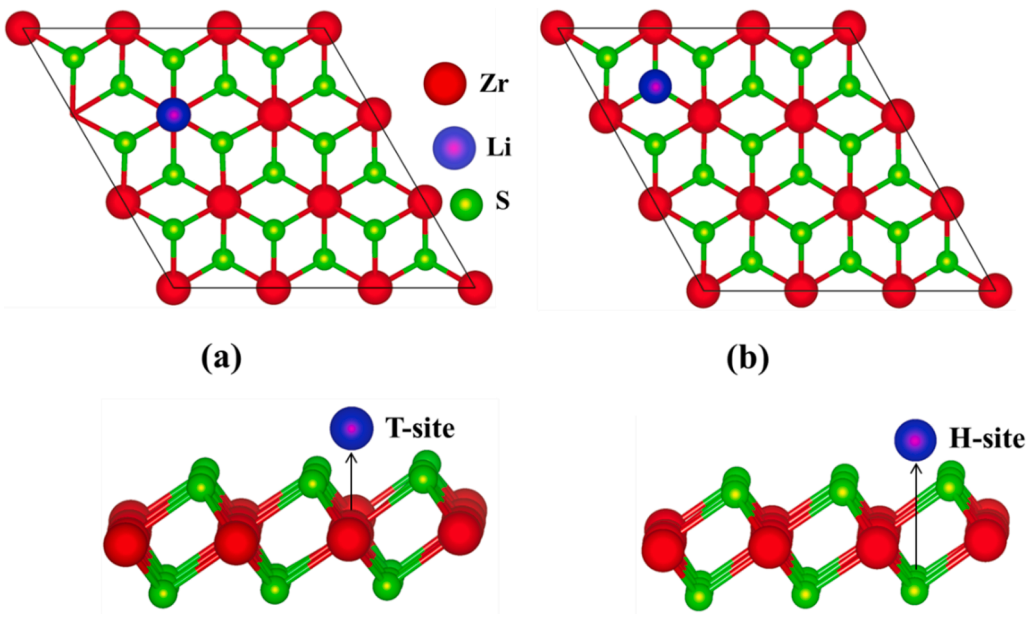

Fig. 1. Ball and stick model of 3 × 3 × 1 supercell of ZrS_2 monolayer with a Li atom adsorbed on (a) T-site and (b) H-site. Upper panel is top view and lower panel is side view.

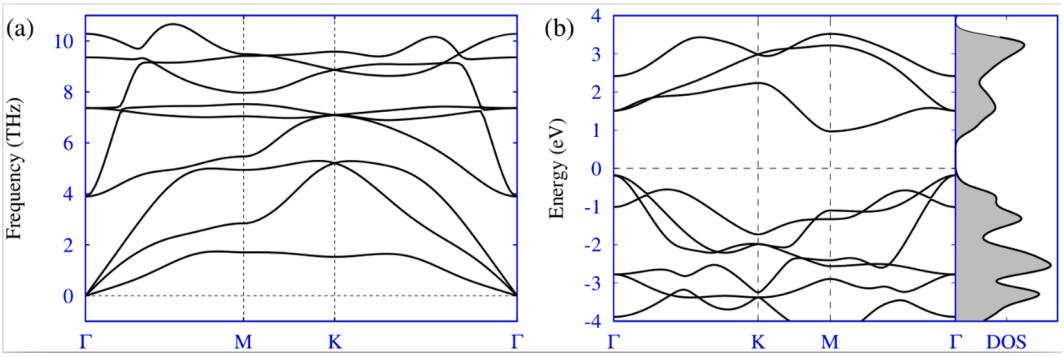

Fig. 2. (a) The phonon (a) and electronic band structures along with TDOS (b) respectively, for the ZrS_2 monolayer in 1T tetragonal prismatic phase.

3.2. Li on ZrS_2 monolayer

3.2.1. Li adsorption

Adsorption and diffusion are two important parameters to measure the suitability of a material as an electrode. Because adsorption energy defines the charge storage capacity and diffusion defines the charge/discharge rate of a battery cell. Therefore, it is necessary to study the adsorption and diffusion of the Li ions on the surface of the monolayer ZrS_2 and graphene individually and then compare it with that of ZrS_2/graphene heterostructure. The Li binding energy with monolayer ZrS_2 is defined as: $E_b = E_{ZrS_2} + E_{Li_{bulk}} - E_{ZrS_2+Li}$ where E_{ZrS_2+Li} is the calculated total energy of the monolayer ZrS_2 with adsorbed Li atoms, E_{ZrS_2} is the total energy of pristine ZrS_2 monolayer and $E_{Li_{bulk}}$ is the total energy of Li in the bulk crystal structure in zinc blend cubic phase. A larger absolute binding energy value means that the configuration (Li adsorbed ZrS_2 monolayer) is stable. This formula is employed to find the most favorable adsorption site for Li on the monolayer ZrS_2. According to the geometry of the ZrS_2 monolayer we consider three possible positions for the adsorption of Li atoms. The first one is the site at the top of the Zr atom, which we call the T-site, the second one is above the hexagon center, which we call the H-site, as shown in Fig. 1(a) and 1(b), respectively. Top of the S atom from the top layer is selected as the third Li adsorption site but due to its high Li adsorption energy this site will not be considered for further calculations. The calculated binding energies for the H and T sites are 1.41 and 1.31 eV, respectively. The binding energies for the Li atom at the H- and T-sites are very close, this is because of the same type of nearest neighbor S atoms and same coordination of Li at the two sites. The structural parameters, electronic charge and binding energy of the Li atoms adsorbed at the H- and T-sites of ZrS_2 monolayer are given in Table 1. Table 1 depicts that the distance between adsorbed Li and S atom ($d_{Li\text{-}S}$) is shorter than the distance between Li and Zr atoms ($d_{Li\text{-}Zr}$). As the S atoms are more electronegative than the Zr atoms, surely the Li atoms will donate their valence electrons to the nearest S atoms to form a strong ionic bond to result in higher binding energy.

To see the effect of Li adsorption concentration on the absolute binding energy we have calculated the binding energy as a function of specific capacity on the surface of 2 × 2 × 1 supercell of ZrS_2 monolayer. The calculated binding energy versus specific capacity curve is plotted in Fig. 3(b). The higher binding energies of the Li adsorption on ZrS_2

Table 1
Structural parameters, binding energy and charge for Li atoms adsorbed on the surface of ZrS_2 surface with 3 × 3 × 1 supercell.

System	d_{Li-Zr} (Å)	d_{Li-S}(Å)	E_b (eV)	Q (|e|)
H-site	3.50	2.37	1.41	0.854
T-site	3.02	2.42	1.31	0.870

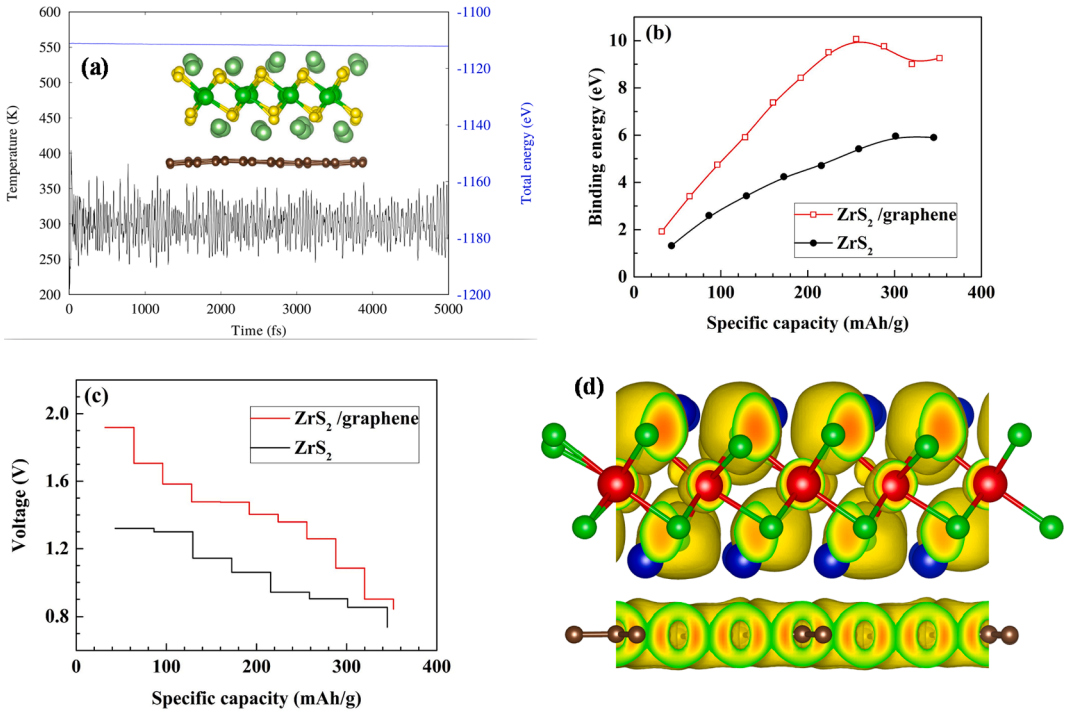

Fig. 3. (a) Ab-initio molecular dynamic simulation for ZrS_2/graphene heterostructure at 500 K; (b) The total binding energy of the Li adsorption on the ZrS_2 monolayer and ZrS_2/graphene heterostructure as a function of specific capacity; (c) The open circuit voltage for ZrS_2 monolayer and ZrS_2/graphene heterostructure as a function of specific capacity; (d) Electron localization function for Li adsorbed ZrS_2/graphene heterostructure, the yellow color shows electron accumulation at the isosphere of 0.6 e/Å^3. (For interpretation of the references to color in this figure legend, the reader is referred to the web version of this article.)

monolayer shows that the configuration (Li adsorbed ZrS_2 monolayer) is stable. The binding energy increases with the Li storage capacity for ZrS_2 monolayer means that the configuration becomes more and more stable. Thus, ZrS_2 monolayer has an excellent response to the Li ion intercalation. The calculated binding energy for the Li adsorption on ZrS_2 surface is much higher than those previously reported for MoS_2, SnS_2 and TiS_2 monolayers [11,12,31]. This fact indicates that ZrS_2 monolayer may play an important role in LIBs while they are not yet achieved experimentally and utilized practically.

To interpret the electron transfer process induced by the Li adsorption on the ZrS_2 monolayer, we have calculated the charge density difference $\Delta\rho = \rho_{ZrS_2+Li} - \rho_{ZrS_2} - \rho_{Li}$, where ρ_{ZrS_2+Li},ρ_{ZrS_2} and ρ_{Li} are the charge densities of Li adsorbed ZrS_2 monolayer, pristine $3 \times 3 \times 1$ ZrS_2 monolayer and isolated Li atoms, respectively. The calculated charge density differences shown in Fig. 4(a) and 4(b) indicate that Li atoms are ionized up on adsorption at the T- and H-sites of the ZrS_2 monolayer to donate their outermost electrons to the ZrS_2 surface. This means that ZrS_2 is useful for the Li adsorption at very low concentration.

3.2.2. *Specific capacity*

The amount of ions stored per unit mass by a battery is termed as specific capacity. Mathematically, it can be defined as, $\chi = nF/N_{ZrS_2}$, where $\chi$is the specific capacity with SI unit of mAh/g, n is the number of Li atoms adsorbed on the surface of ZrS_2 monolayer with $2 \times 2 \times 1$ supercell, F is the Faradays constant (26,801 mAh/mol) and N_{ZrS_2} is the molar mass of ZrS_2 monolayer. The reversible reaction at anode can be

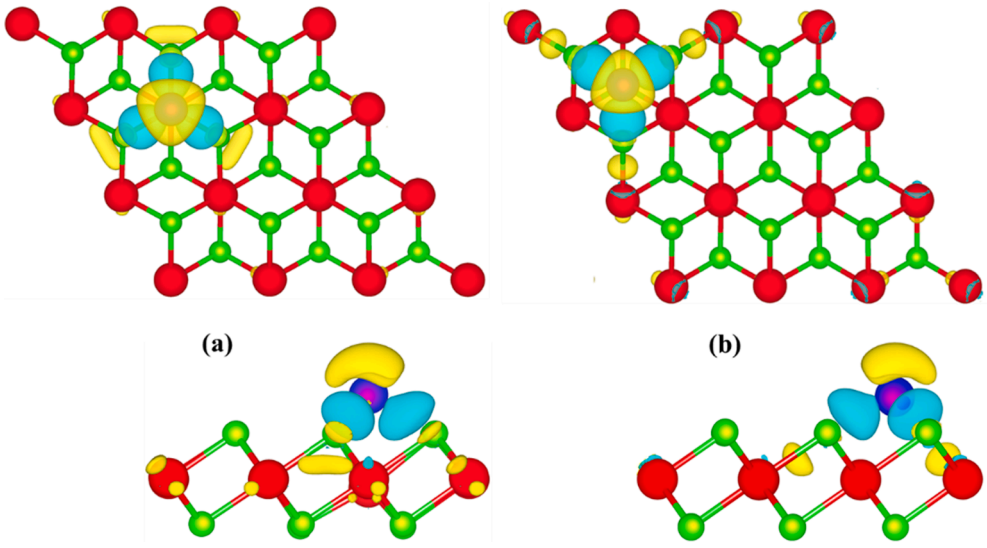

Fig. 4. (a) The charge density difference for the Li adsorption at the T-site of ZrS_2 monolayer; (b) The charge density difference for the Li adsorption at the H-site of ZrS_2 monolayer. Upper panel is top view and lower panel is side view. Electron gain upon the Li adsorption is indicated with yellow color at the isosurface of -0.00189 eÅ^{-1} and electron loss in the light blue at an isosurface of 0.00189 eÅ^{-1}. (For interpretation of the references to color in this figure legend, the reader is referred to the web version of this article.)

written as: $Li_x + xe^- + ZrS_2 \square Li_xZrS_2$. Thus by filling the available H sites only, the capacity of the ZrS_2 based on the given formula comes out to be 350 mAh/g to make a composition Li_2ZrS_2. However, the Li binding energy allows us to fill all the T-sites as well, the Li storage capacity thus becomes double (700 mAh/g) leading to Li_4ZrS_2 composition. However, high Li load causes the ZrS_2 decomposition in Li_2S and Zr. The Li storage capacity are reported as 372 mAh/g, for graphite, 340 mAh/g for bulk MoS_2, 300 mAh/g for MoS_2 bilayer, while it is in the range of 146–352 mAh/g for 2D TMDs, Mxenes, and carbides [19,58–61]. The theoretical calculated storage capacity for Sc_2C (Mxene) and some other functionalized Mxenes are 462 mAh/g and 320 mAh/g [62,63]. Thus, the value of the calculated maximum specific capacity for ZrS_2 monolayer is much higher than the reported stable 2D materials. The flow of Li ions in the battery between the cathode and anode can be written in the form of a chemical reaction as, $xLi^+ + xe^- + ZrS_2 \rightleftharpoons Li_xZrS_2$, electrons produced in this reaction flow in the outer circuit while the positive Li ions move inside the battery between the two electrodes. To have a high reversibility and high charge/discharge rate, electrode material of the battery should be metallic. Our results show that the pristine ZrS_2 is semiconducting but the Lithiated one is metallic. 100% reversibility of the Li ions for such a material is not possible, that is one of the reasons to prefer the ZrS_2/graphene heterostructure over ZrS_2 monolayer as anode material. Also, the decomposition of ZrS_2 monolayer at high Li concentration asks for ZrS_2/graphene heterobilayer.

3.2.3. Open circuit voltage

Open circuit voltage (OCV) is a key parameter to determine the performance of an electrode material. Electrode materials with low OCV are the best fit for anodic applications in the rechargeable LIBs. Therefore, we calculate the OCV by the equation, $\varepsilon_{OCV} = -(E_{ZrS_2+Li_n} - E_{ZrS_2} - nE_{Li_{bulk}})/ne$, where $E_{ZrS_2+Li_n}$ is the total energy of ZrS_2 monolayer with nLi ions adsorbed at the H site, and

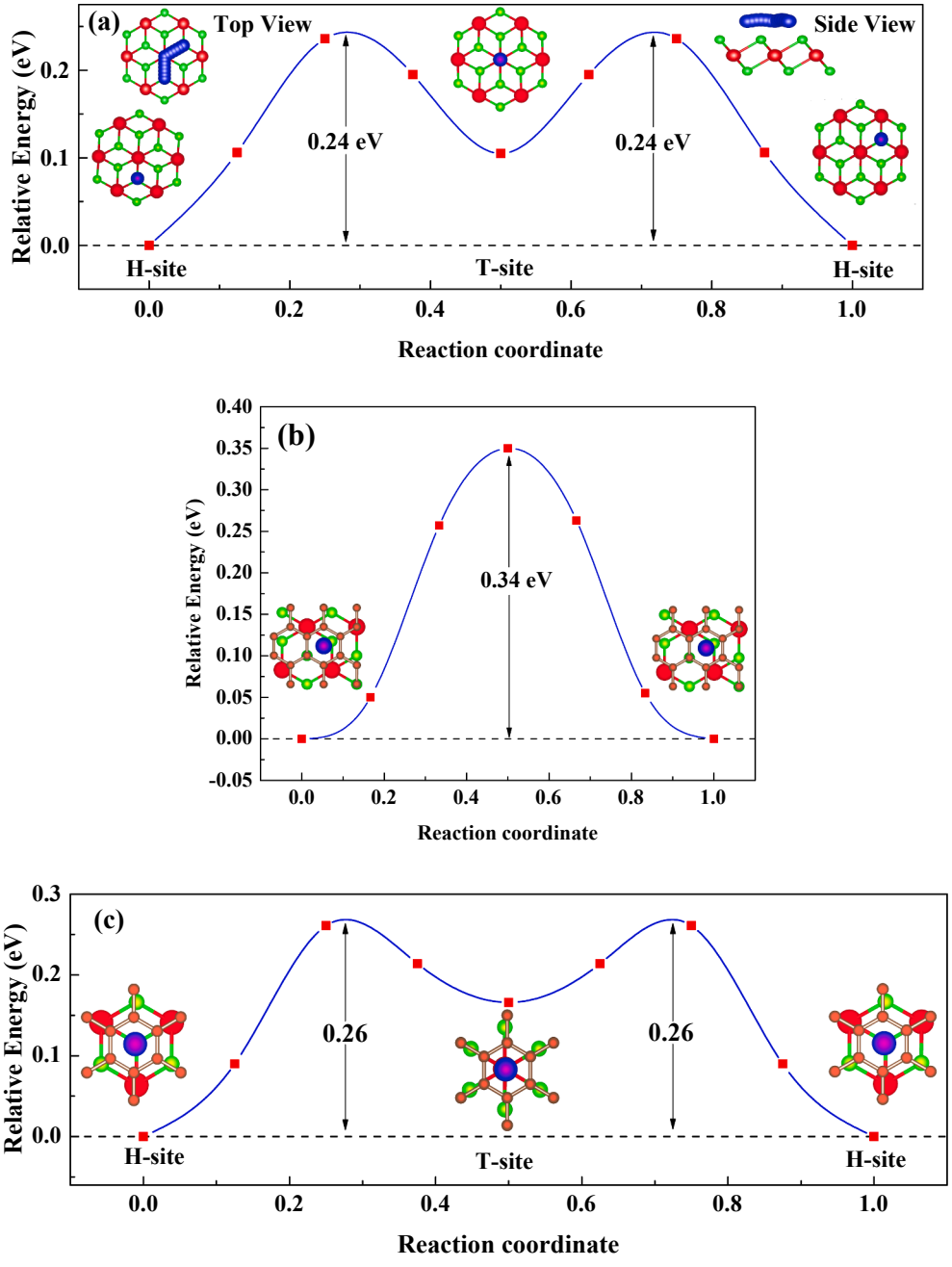

Fig. 5. Minimum energy path for the diffusion of Li atom from one H-site to an adjustment H-site through T-site; (a) on the surface of ZrS_2 monolayer with activation energy barrier of 0.24 eV; (b) on the surface of graphene from one adjacent site to another adjacent in the ZrS_2/graphene heterostructure with activation energy barrier 0.34 eV; (c) on the surface of ZrS_2 monolayer in the ZrS_2/graphene heterostructure with activation energy barrier of 0.26 eV. The insets in the graph show the trajectory of Li along the H–T–H path.

E_{ZrS_2} and $E_{Li_{bulk}}$ are the total energies of pristine ZrS_2 monolayer and a Li atom in its bulk crystal structure, respectively. OCV has been estimated by this formula for all the Li ions concentrations adsorbed on the surface of ZrS_2 monolayer as shown in Fig. 3(c). It decreases with increasing the specific capacity and drop to 0.7 V at the maximum specific capacity of 350 mAh/g. The OCV values reported for monolayers, VS_2, Mo_2C, W_2C and SnS_2, are 0.92, 0.84, 0.7 and 1 V, respectively. It is also reported that the average OCV should be lower than 0.8 V for a commercial anode and should be greater than zero to avoid the dendrite formation [5,12,19,28]. The calculated average electrode potential is 0.51 V and 0.22 V for different chemical stoichiometry for the Li adsorbed $NbSe_2$ monolayer. Thus, the average open circuit of 0.7 V for the Li atoms on the ZrS_2 monolayer is pretty good to be used for commercial purposes.

3.2.4. Li diffusion

One of the most required properties of an electrode material is its high Li mobility which allows the easy flow of Li currents inside the anode material. Therefore, we consider the Li ion diffusion at the surface of the ZrS_2 monolayer and related diffusion barrier. Here we consider energetically the most favorable path for the migration of Li ions, i.e. from one H-site to an adjacent H-site through the intermediate T-site and their migration pathway is optimized with the NEB model. The relative energy profile against the reaction coordinates between the adjacent H-sites is shown in Fig. 5(a). Here red square data points on the curve represent the relative energy along the reaction path with respect to the H-site. Our investigated MEP for the diffusion of Li ion, migrated from the H-site to the nearby H-site through a T-site has a zigzag curve shape path with migration energy barrier of 0.24 eV. Being the energy difference of the highest energy point on the MEP and the reference point (H-site), it is also called the activation energy barrier or diffusion barrier. The calculated activation energy barrier for ZrS_2 monolayer is much lower than that of pristine graphene and pristine Si, and is comparable to other TMDs [41,43,64–67].

4. Li insertion into ZrS_2/graphene heterostructure

4.1. Li adsorption

The $2 \times 2 \times 1$ supercell of ZrS_2 monolayer and $3 \times 3 \times 1$ supper cell of graphene were combined to form the ZrS_2/graphene heterostructure. Its stacking stability was confirmed with the stacking energy per atom defined as, $E_f = -\left(E_{ZrS_2/graphene} - E_{ZrS2} - E_{graphene}\right)/n$, where $E_{ZrS_2/graphene}$, E_{ZrS2} and $E_{graphene}$ are the total energies of ZrS_2/graphene heterostructure, $2 \times 2 \times 1$ ZrS_2 supercell and $3 \times 3 \times 1$ graphene supercell, respectively. The calculated formation energy for ZrS_2/graphene heterostructure is 0.21 eV/atom. The small amount of stacking energy in the ZrS_2/graphene heterostructure is due to the week van der Waal interactions. The stacking energy is 0.12 eV/atom for SnS_2/graphene, 0.03 eV/atom for MoS_2/graphene and 0.189 eV/atom for MoS_2/VS_2 heterostructures [12,42,68]. Thus, the formation energy of 0.21 eV/atom for ZrS_2/graphene is slightly higher than those predicted heterostructures, showing a more stable stacking compared to the other heterostructures. Furthermore, we checked out the thermal stability for the maximum Li adsorbed ZrS_2/graphene heterostructure with ab-initio molecular dynamics (MD) simulation at 500 K. The MD simulation was carried out in the canonical (NVT) ensemble using a Nosé thermostat [52]. Fig. 3(a) displays the relationship between temperature, total energy and simulation time. Obviously, there is no structural reconstruction in the ZrS_2/graphene heterostructure (Fig. 3a), and the amplitude of total energy fluctuation is small during the MD simulation, demonstrating that the ZrS_2/graphene heterostructure is thermally stable. The Li atoms fluctuate from the favorable adsorption position due to thermal agitation and reconstruct the initial stable geometry. The equilibrium interlayer distance is 3.2 Å from the top S atoms to the graphene and 4.5 Å from the Zr atoms, which are comparable with the reported theoretical calculations on graphene based composite [12]. Thus, the ZrS_2/graphene heterostructure also provide sufficient free space for the Li insertion. Regarding the energetic stability, we have considered three positions for the adsorption of Li on the outside surface of ZrS_2, interface of ZrS_2/graphene heterostructure, and surface of the graphene and at the interface. The H-site and T-site at the interface are found to be the most favorable sites for the adsorption. While on the pure graphene surface the center of hexagon (G_{cent}) formed by the C atoms is the most favorable position for the adsorption of Li. The calculated binding energy E_b at the center of graphene ring and the charge transferred from Li to graphene are −0.553 eV and 0.03 |e|, respectively. This means that pure graphene is not suitable for the LIBs as an anode material; this is in good agreement with the previous theoretical calculations [12,59]. On the other hand, the binding energy for the Li adsorption on the surface of graphene in the ZrS_2/graphene heterostructure is 0.1 eV as shown in Table1. This higher binding strength shows that Li can be stored above the center of graphene ring (G_{cent}) without the formation of metallic cluster. The higher binding strength in the heterostructure comes from the Li interaction with the S atoms (nearest neighbors). While for the other two positions the C-C bond length and the position on the top of C atoms are unfavorable for the Li adsorption.

The adsorption of Li on the surface of ZrS_2 in the heterostructure case is similar to the Li adsorption on the pristine ZrS_2. The Li atom prefers the H-site (H_s) and T-site (T_s) on the surface of ZrS_2 in the ZrS_2/graphene heterostructure. The calculated binding energies for these sites are given in Table 2, which are close to those for the same sites on the pristine ZrS_2 monolayer. This is because the graphene layer is very far from the adsorbed Li atoms. In the interface of the heterostructure the Li atoms prefer to be at the H-site and T-site, but the calculated binding energies at different H-sites and T-sites are slightly different. In Table 2 the considered favorable H-sites are H1, H2, H3, and H4 with corresponding binding energies of 1.91, 1.54, 1.54 and 1.92 eV, respectively; while the favorable T-sites are T1, T2, T3 and T4 with corresponding binding energies of 1.4, 1.87, 1.4 and 1.75 eV, respectively. The difference in the binding energy is due to the different C atom surroundings at the T- and H-sites at the interface of ZrS_2/graphene composite. The binding energies of Li at the interface are higher than that on the ZrS_2 surface. This is because the Li at the interface interacts with both ZrS_2 monolayer and graphene. The binding energy results are similar to the reported ones of Li adsorption in the heterostructure composed of graphene and phosphorene [6,12]. In addition, we have also calculated the charge transfer at these favorable sites by Bader charge analysis, and, the results are quite similar to that of ZrS_2 monolayer case as shown in Table 2, which means that the Li atoms adsorbed at these sites form strong covalent bonds and they are energetically stable. The electron localization function (ELF) calculations in Fig. 3(d) for Li intercalated ZrS_2/graphene heterobilayer depicts that the charge between Li and S has a high tendency towards S. It means that even at high Li concentration the Li preserves its ionic character. The relaxation distances of the Li at these sites from the S atom, d_{Li-S} (Å), are also shown in Table 2.

The binding energy with respect to specific capacity was studied and the results are given in Fig. 3(b). The binding energy increase with increasing the Li content, then the Li atom intercalation to the heterostructure becomes stronger with increasing the Li amount in the ZrS_2/graphene heterostructure. Also, the values of binding energy in heterostructure case are higher than the pristine ZrS_2 case. The higher values of the binding energy for the ZrS_2/graphene heterostructure indicate that it can have more Li storage capacity than that of ZrS_2 monolayer. Our calculated binding energy values are much higher than those reported for other heterostructures [6,11,12,31,42,43].

4.2. Open circuit voltage and specific capacity

The OCV versus specific capacity curve is shown in Fig. 3(c); the OCV decreases down to 0.8 V with increasing the capacity of the Li content in the ZrS_2/graphene heterostructure, a suitable open circuit voltage for

Table 2
Structural parameters, binding energy and charge for Li atoms adsorbed at the H-sites of the interface (H1, H2, H3, H4), T-sites of the interface (T1, T2, T3, T4), an H-site of ZrS_2 surface (H_s-site) and a T-site of ZrS_2 surface (T_s-site) and the position above the center of graphene ring (G_{cent}) of the ZrS_2/graphene heterostructure.

system	H1	H2	H3	H4	T1	T2	T3	T4	H_s	T_s	G_{cent}
d_{Li-S} (Å)	2.49	2.50	2.49	2.39	2.43	2.52	2.43	2.47	2.36	2.41	4.5
E_b(eV)	1.91	1.54	1.54	1.92	1.40	1.87	1.40	1.75	1.41	1.37	0.1
Q ($\|e\|$)	0.864	0.861	0.864	0.861	0.873	0.870	0.873	0.870	0.864	0.873	0.898

practical application [6,12,28,68]. Furthermore, we also studied the highest possible storage capacity of the ZrS_2/graphene heterostructure and maximum capacity of 380 mAh/g can be achieved, which is higher than the 350 mAh/g for the pristine ZrS_2 monolayer. Thus, the specific capacity of ZrS_2 monolayer can be improved when interfaced with graphene.

4.3. Li diffusion in ZrS_2/graphene heterostructure

As we have discussed earlier that high power rate is the demand of a second generation battery, which can be defined by the Li ion mobility of the electrode material. Therefore, it is necessary to evaluate minimum energy path (MEP) and diffusion energy barrier to the flow of Li in the ZrS_2/graphene heterostructure. Thus, we have employed the NEB model to calculate the MEP and activation energy barrier for the flow of Li ions in the ZrS_2/graphene heterostructure. We consider three possible pathways for the diffusion of Li atoms: (1) on the outer surface of ZrS_2, (2) the outer surface of graphene, and (3) the interface of the ZrS_2/graphene heterostructure. We first studied the diffusion of Li atom on the ZrS_2 surface in the heterostructure by considering the energetically favorable sites, i.e. from the H-site to a nearby H-site through the T-site, which is similar to the pristine ZrS_2 monolayer case. The diffusion energy path is also in the same zigzag shape, but the diffusion barrier is slightly increased to 0.26 eV, as shown in Fig. 5(c). The Li atoms move on the outer surface of ZrS_2 in ZrS_2/graphene heterostructure feel negligible effect of the graphene layer. In the second case when the Li atoms move on the outer surface of the graphene and diffuses between the two adjacent sites, i.e. moving from the center of a graphene ring to the center of a nearby graphene ring passing through the C-C bridge, the calculated barrier is 0.34 eV as shown in Fig. 5(b), which is comparable with the barrier for graphene surface in phosphorene/graphene heterostructure [6]. Finally, the diffusion energy barrier at the interface of ZrS_2/graphene heterostructure is shown in Fig. 6. Among the four H-sites and four T-sites, we consider H1 site as a reference site because it is the most favorable site; the calculated energy barrier is increased to 0.286 eV, which is near to the theoretical predicted barrier of SnS_2/graphene heterostructure [12].

5. Electronic structure of ZrS_2 monolayer and ZrS_2/graphene heterostructure

Further to see the effects of Li adsorption on the electronic structure of ZrS_2 monolayer and ZrS_2/graphene heterostructure, we have investigated the electronic structures in the term of TDOS as shown in Fig. 7. The ZrS_2 monolayer is semiconductor with the energy gap of 1.12 eV (Fig. 7(a)), but with the Li adsorption its band gap decreases and become a metal when Li atoms cover all the available sites and reached to its maximum storage capacity, as shown in Fig. 7(b). When increasing the Li concentration the TDOS intensity at the Fermi level increases and ZrS_2 monolayer becomes more conductive and hence the electrical conductivity of ZrS_2 monolayer increases. Previously investigated materials like graphene and MoS_2 are insulator and semiconductor, respectively, and have intrinsically low conductivity. Although some strategies like doping can be used to make these materials metallic, but this will

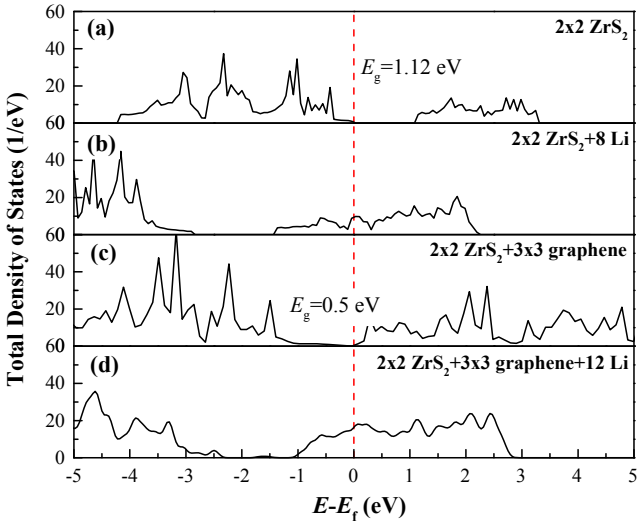

Fig. 7. Total density of states (TDOS) for: (a) pristine ZrS_2 monolayer; (b) Li adsorbed ZrS_2 monolayer; (c) ZrS_2/graphene heterostructure; (d) Li adsorbed ZrS_2/graphene heterostructure. In Fig. 7(c) change the Eg = 0.5 to 0.

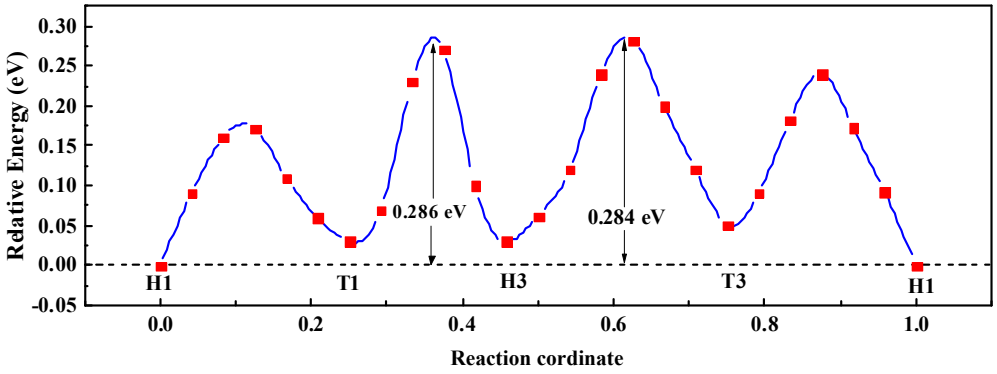

Fig. 6. Minimum energy path for the diffusion of Li at the interface of ZrS_2/graphene heterostructure with activation energy barrier 0.286 eV.

increase the diffusion barrier and will make electrode materials costly. When ZrS_2 monolayer is interfaced with graphene, its band gap decreases to 0.5 eV; by further increasing the Li concentration the ZrS_2/graphene heterostructure becomes metallic (Fig. 7(d)) and thus reaches the requirement of high electronic conductivity. Thus, both ZrS_2 monolayer and ZrS_2/graphene heterostructure show metallic characteristic before reaching to their maximum storage capacity as desirable for the high performance electrodes. The tendency of our calculated electronic structure for ZrS_2 monolayer and ZrS_2/graphene heterostructure are consistent with reported theoretical calculations [6,11,12,28,70,71].

Finally, we want to comment on the experimental authenticity of our work. Although, the ZrS_2/graphene heterobilayer system may not be used as anode in Li ion batteries, few layer ZrS_2 with graphene insertion may be used as anode. Also, it may not be possible to grow the pristine ZrS_2 layer on graphene without defects. But ZrS_2 nanoflakes, nanoplates, or few layers ZrS_2 with some defects may be possible. Our atomistic report on the hybrid ZrS_2/graphene system concludes that the graphene in this system will provide mechanical strength and electronic conductivity while the ZrS_2 will provide a strong binding to host Li ions.

6. Conclusion

Using density functional theory, the electrochemical properties of ZrS_2 monolayer and ZrS_2/graphene heterobilayer have been studied for applications in rechargeable LIBs. The energetic and dynamic stabilities of these materials have been confirmed first and lithaited then. The low Li diffusion barrier (0.24 eV), low half-cell voltage (0.7 V) and high storage capacity (700 mAh/g) of monolayer ZrS_2 make it a prospective anode material for the LIBs. Its high energy gap and decomposition at high Li adsorption can reduce its reversibility but this issue can be overcome by making its contact with graphene. A significant improvement in the Li binding energy of the ZrS_2/graphene heterobilayer has been noticed compared to that graphene and monolayer ZrS_2. The open circuit voltage for the Li adsorbed ZrS_2/graphene heterobilayer is found to be 0.8 eV, which is suitable voltage for practical anode materials. The calculated diffusion barrier for the Li atoms in the case of ZrS_2/graphene heterostructureis 0.286 eV, hence the Li ions can easily flow in the ZrS_2/graphene heterobilayer; this will give high conductivity as desirable for an efficient LIB. The TDOS results show that ZrS_2 monolayer is insulating while the ZrS_2/graphene heterobilayer is metallic. Thus the ZrS_2 monolayer and graphene properties can be utilized in the ZrS_2/graphene heterobilayer to manufacture a high efficient anode material for LIBs.

CRediT authorship contribution statement

Shafiq Ur Rehman: Conceptualization, Methodology, Investigations, Software, Writing original draft. **Abdus Samad:** Software, Calculations, Writing - review & editing. **Muhammad Saeed**: Formal analysis. **Bin Amin:** Discussion and Revision. **Muhammad Hafeez:** Formal analysis. **Irshad A Mir:** Discussion and Revision. **ling Zhu:** Supervision and Resources.

Declaration of Competing Interest

The authors declare that they have no known competing financial interests or personal relationships that could have appeared to influence the work reported in this paper.

Acknowledgement

This work was financially supported by the grants from the Science and Technology Innovation Commission of Shenzhen (Grant no: JCYJ20180305125302333, ZDSYS201707271554071) and Shenzhen University fund (No. 2017007).

References

[1] Y. Shi, L. Wen, G. Zhou, J. Chen, S. Pei, K. Huang, H.-M. Cheng, F. Li, 2D Mater. 2 (2015) 024004–24008.
[2] N.K. Jena, R.B. Araujo, V. Shukla, R. Ahuja, ACS Appl. Mater. Interf. 9 (2017) 16148–16158.
[3] G. Yuan, T. Bao, X. Qi, P.F. Liu, Z. Huang, B.T. Wang, Appl. Surf. Sci. 480 (2019) 448–453.
[4] C. Mücksch, H.M. Urbassek, J. Phys. Chem. B 120 (2016) 7889–7895.
[5] C. Mücksch, C. Rösch, C. Müller-Renno, C. Ziegler, H.M. Urbassek, J. Phys. Chem. C 119 (2015) 12496–12501.
[6] G.-C. Guo, D. Wang, X.-L. Wei, Q. Zhang, H. Liu, W.-M. Lau, L.-M. Liu, J. Phys. Chem. Lett. 6 (2015) 5002–5008.
[7] Y. Xie, Y. Dall'Agnese, M. Naguib, Y. Gogotsi, M.W. Barsoum, H.L. Zhuang, P. R. Kent, ACS Nano 8 (2014) 9606–9615.
[8] A. Samad, H.J. Kim, Y.-H. Shin, Appl. Surf. Sci. 475 (2019) 151–157.
[9] D. Li, X. Chen, P. Xiang, H. Du, B. Xiao, Appl. Surf. Sci. 501 (2020) 144221–144222.
[10] D. Dubal, O. Ayyad, V. Ruiz, P. Gomez-Romero, Chem. Soc. Rev. 44 (2015) 1777–1790.
[11] A. Samad, A. Shafique, Y.-H. Shin, Nanotech. 28 (2017) 175401–175407.
[12] A. Samad, M. Noor-A-Alam, Y.-H. Shin, J. Mater. Chem. A 4 (2016) 14316–14323.
[13] Q. Peng, X. Sun, H. Wang, Y. Yang, X. Wen, C. Huang, S. Liu, S. De, Appl. Mater. Today 7 (2017) 169–178.
[14] B.A. Korgel, J. Phys. Chem. Lett. 5 (2014) 74–750.
[15] Y. Xiao, J.-Y. Hwang, Y.-K. Sun, J. Mater. Chem. A 4 (2016) 10379–10393.
[16] H. Zhang, M. Zhang, M. Zhang, L. Zhang, A. Zhang, Y. Zhou, P. Wu, Y. Tang, J. Colloid Interf. Sci. 501 (2017) 267–272.
[17] M. Moura, R. Barrada, J. Almeida, T. Moreira, M. Schettino, J. Freitas, S. Ferreira, M. Lelis, M. Freitas, Chemosphere 182 (2017) 339–347.
[18] J. Li, S. Xiong, Y. Liu, Z. Ju, Y. Qian, ACS Appl. Mater. Interf. 5 (2013) 981–988.
[19] A. Samad, A. Shafique, H.J. Kim, Y.-H. Shin, J. Mater. Chem. A 5 (2017) 11094–11099.
[20] W. Yuan, Y. Zhang, L. Cheng, H. Wu, L. Zheng, D. Zhao, J. Mater. Chem. A 4 (2016) 8932–8951.
[21] K.F. Mak, C. Lee, J. Hone, J. Shan, T.F. Heinz, Phys. Rev. Lett. 105 (2010) 136805–136814.
[22] Y.Y. Wu, T. Bo, X. Zhu, Z. Wang, J. Wu, Y. Li, B.T. Wang, Appl. Surf. Sci. 513 (2020) 145821–145829.
[23] S. Tongay, H. Sahin, C. Ko, A. Luce, W. Fan, K. Liu, J. Zhou, Y.-S. Huang, C.-H. Ho, J. Yan, Nat. Commun. 5 (2014) 3252–3256.
[24] F.A. Rasmussen, K.S. Thygesen, J. Phys. Chem. C 119 (2015) 13169–13183.
[25] F. Li, Y. Qu, M. Zhao, J. Mater. Chem. A 4 (2016) 8905–8912.
[26] X. Zhang, C. Yang, Y. Pan, M. Weng, L. Xu, S. Liu, J. Yang, J. Yan, J. Li, B. Shi, J. Yang, J. Zheng, F. Pan, J. Lu, J. Mater. Chem. A 7 (2019) 14042–14050.
[27] S.U. Rehman, B. Amin, M. Hafeez, S.A. Khan, I.A. Mir, W. Uddin, L. Wei, L. Zhu, Appl. Surf. Sci. 505 (2020) 144530–144539.
[28] Y. Jing, Z. Zhou, C.R. Cabrera, Z. Chen, J. Phys. Chem. C 117 (2013) 25409–25413.
[29] Y. Huang, C. Ling, X. Chen, D. Zhou, S. Wang, RSC Adv. 5 (2015) 32505–32510.
[30] D. Wang, L.-M. Liu, S.-J. Zhao, Z.-Y. Hu, H. Liu, J. Phys. Chem. C 120 (2016) 4779–4788.
[31] F. Ersan, G.k. Gökoğlu, E. Aktürk, J. Phys. Chem. C 119 (2015) 28648–28653.
[32] L. Jiang, B. Lin, X. Li, X. Song, H. Xia, L. Li, H. Zeng, ACS Appl. Mater. Interf. 8 (2016) 2680–2687.
[33] G. Du, Z. Guo, S. Wang, R. Zeng, Z. Chen, H. Liu, Chem. Commun. 46 (2010) 1106–1108.
[34] H. Hwang, H. Kim, J. Cho, Nano Lett. 11 (2011) 4826–4830.
[35] Y. Li, D. Wu, Z. Zhou, C.R. Cabrera, Z. Chen, J. Phys. Chem. Lett. 3 (2012) 2221–2227.
[36] E. Pomerantseva, Y. Gogotsi, Nat. Energy 2 (2017) 17089–17096.
[37] Y. Fang, Y. Lv, F. Gong, A.A. Elzatahry, G. Zheng, D. Zhao, Adv. Mater. 28 (2016) 9385–9390.
[38] Y. Su, S. Li, D. Wu, F. Zhang, H. Liang, P. Gao, C. Cheng, X. Feng, ACS Nano 6 (2012) 8349–8356.
[39] Y. Guan, B. Xu, Appl. Surf. Sci. 481 (2019) 1459–1465.
[40] C. Zhao, X. Wang, J. Kong, J.M. Ang, P.S. Lee, Z. Liu, X. Lu, ACS Appl. Mater. Interf. 8 (2016) 2372–2379.
[41] L. Shi, T. Zhao, A. Xu, J. Xu, J. Mater. Chem. A 4 (2016) 16377–16382.
[42] A. Samad, Y.-H. Shin, ACS Appl. Mater. Interf. 9 (2017) 29942–29949.
[43] N.S. Mikhaleva, M. Visotin, A.A. Kuzubov, Z.I. Popov, J. Phys. Chem. C 121 (2017) 24179–24184.
[44] M. Zhang, Y. Zhu, X. Wang, Q. Feng, S. Qiao, W. Wen, Y. Chen, M. Cui, J. Zhang, C. Cai, J. Am. Chem. Soc. 137 (2015) 7051–7054.
[45] Y. Li, J. Kang, J. Li, RSC Adv. 4 (2014) 7396–7401.
[46] L. Ao, A. Pham, H. Xiao, X. Zu, S. Li, PCCP 18 (2016) 25151–25160.
[47] Z. Zeng, Z. Yin, X. Huang, H. Li, Q. He, G. Lu, F. Boey, H. Zhang, Ang. Chem. Inter. Ed. 50 (2011) 11093–11097.
[48] S.U. Rehman, Z. Ding, PCCP 20 (2018) 16604–16614.
[49] X. Zhang, Z. Meng, D. Rao, Y. Wang, Q. Shi, Y. Liu, H. Wu, K. Deng, H. Liu, R. Lu, Energy Environ. Sci. 9 (2016) 841–849.
[50] G. Kresse, J. Furthmüller, Phys. Rev. B 54 (1996) 11169–11181.
[51] J.P. Perdew, K. Burke, M. Ernzerhof, Phys. Rev. Lett. 77 (1996) 3865–3868.
[52] J. Paier, M. Marsman, K. Hummer, G. Kresse, I.C. Gerber, J.G. Ángyán, J. Chem. Phys. 124 (2006) 154709–154713.
[53] H.J. Monkhorst, J.D. Pack, Phys. Rev. B 13 (1976) 5188–5192.
[54] S. Grimme, J. Comput. Chem. 25 (2004) 1463–1473.

[55] R. Olsen, G. Kroes, G. Henkelman, A. Arnaldsson, H. Jónsson, J. Chem. Phys. 121 (2004) 9776–9792.
[56] G. Henkelman, B.P. Uberuaga, H. Jónsson, J. Chem. Phys. 113 (2000) 9901–9904.
[57] A. Togo, F. Oba, I. Tanaka, Phys. Rev. B 78 (2008) 134106–134109.
[58] G.J. Martyna, M.L. Klein, M. Tuckerman, J. Chem. Phys. 97 (4) (1992) 2635.
[59] C. Ling, F. Mizuno, PCCP 16 (2014) 10419–10424.
[60] J.B. Goodenough, Y. Kim, Chem. Mater. 22 (2009) 587–603.
[61] D. Er, J. Li, M. Naguib, Y. Gogotsi, V.B. Shenoy, ACS Appl. Mater. Interf. 6 (2014) 11173–11179.
[62] X. Lv, W. Wei, Q. Sun, L. Yu, B. Huang, Y. Dai, ChemPhysChem 18 (2017) 1627–1634.
[63] Z. Zhou Tang, P. Shen, J. Am. Chem. Soc. 134 (2012) 16909–16916.
[64] G.A. Tritsaris, E. Kaxiras, S. Meng, E. Wang, Nano Lett. 13 (2013) 2258–2263.
[65] X. Fan, W. Zheng, J.-L. Kuo, ACS Appl. Mater. Interf. 4 (2012) 2432–2438.
[66] E. Yang, H. Ji, Y. Jung, J. Phys. Chem. C 119 (2015) 26374–26380.
[67] J. Su, Y. Pei, Z. Yang, X. Wang, RSC Adv. 4 (2014) 43183–43188.
[68] X. Shao, K. Wang, R. Pang, X. Shi, J. Phys. Chem. C 119 (2015) 25860–25867.
[70] Q. Peng, Z. Wang, B. Sa, B. Wu, Z. Sun, ACS Appl.Mater. Interf. 8 (2016) 13449–13457.
[71] V.V. Kulish, O.I. Malyi, C. Persson, P. Wu, PCCP 17 (2015) 13921–13928.